

Cite this article as: Wang Shunping, Li Chunyan, Li Jinling, et al. Effect of Tm on Mechanical and Corrosion Properties of Zr-Based Bulk Metallic Glasses[J]. Rare Metal Materials and Engineering, 2021, 50(09): 3076-3084.

ARTICLE

Effect of Tm on Mechanical and Corrosion Properties of Zr-Based Bulk Metallic Glasses

Wang Shunping^{1,2}, Li Chunyan^{1,2}, Li Jinling¹, Wang Haibo¹, Kou Shengzhong^{1,2}

¹ State Key Laboratory of Advanced Processing and Recycling of Nonferrous Metals, Lanzhou University of Technology, Lanzhou 730050, China; ² School of Materials Science and Engineering, Lanzhou University of Technology, Lanzhou 730050, China

Abstract: A series of $(\text{Zr}_{0.6336}\text{Cu}_{0.1452}\text{Ni}_{0.1012}\text{Al}_{0.12})_{100-x}\text{Tm}_x$ ($x=0\sim 5$, at%) bulk metallic glass (BMG) alloys were fabricated by copper mold suction casting, and the effect of Tm on the mechanical and corrosion properties were investigated. The results show that when Tm content increases to 3at%, the glass forming ability (GFA) and compressive plasticity are significantly improved, whereas GFA is decreased by adding excessive Tm. The maximum supercooled liquid region width (ΔT_x) of the alloy with $x=3$ is 100 K, the compressive fracture strength is 1669 MPa, and the plastic strain is 21.01%, which are much higher than those of the $\text{Zr}_{0.6336}\text{Cu}_{0.1452}\text{Ni}_{0.1012}\text{Al}_{0.12}$ BMG (67 K, 1439 MPa, and 5.90%). However, the electrochemical test results show that the alloy with $x=3$ does not have excellent corrosion resistance in 3.5wt% NaCl solution, and the change trend of corrosion resistance and mechanical properties with Tm content is different from the expectation. The possible reason is that the excessive addition of rare-earth element Tm easily causes more oxides, which leads to the severe pitting corrosion. Further addition of Tm can improve the integrity and pitting corrosion resistance of Zr-based BMG passivation film, but the mechanical properties are not ideal.

Key words: Zr-based metallic glass; mechanical properties; corrosion resistance; Tm

The application of bulk metallic glass (BMG) for sensors or spacecraft requires that the materials should have the unique mechanical properties and superior corrosion resistance. Compared with conventional crystalline material, BMG has high strength, high hardness, and excellent corrosion resistance, which has attracted great attention^[1]. However, the plasticity of BMG at room temperature is relatively low, which restricts its wide application as a structural material. Therefore, how to improve the plasticity of BMG becomes the research focus. It is reported that the addition of minor rare-earth elements can improve the room temperature plasticity, glass-forming ability (GFA), and thermal stability of BMG^[2,3]. Many studies have shown that when the Er content of $(\text{Zr}_{65}\text{Cu}_{17.5}\text{Ni}_{10}\text{Al}_{7.5})_{98}\text{Er}_2$ amorphous alloy reaches 2at%, its supercooled liquid region width (ΔT_x) and plastic strain ($\Delta L/L_0$) increase by 11 K and 40%, respectively^[3]. In recent years, the room temperature plastic materials $\text{Zr}_{63.5-x}\text{Hf}_x\text{Al}_9\text{Fe}_{4.5}\text{Cu}_{23}$ ($x=3.0$) with critical diameter d_{\max} of 1 cm have been investigated^[4,5]. It is also reported that the maximum entropy

change δ_{sm} of $\text{Tm}_{39}\text{Ho}_{16}\text{Co}_{20}\text{Al}_{25}$ metallic glass reaches $18.3 \text{ J}\cdot\text{kg}^{-1}\cdot\text{K}^{-1}$ when the magnetic field strength is 5 T, which is larger than that of any previously reported metallic glasses and comparable to that of $\text{Gd}_5\text{Si}_2\text{Ge}_2$ compound with magnetocaloric effect^[6]. There are many reports about the effect of Tm addition on the magnetocaloric effect of metallic glass^[7,8] and high entropy amorphous alloy^[9]. In the meantime, minor alloying method is beneficial to improving the corrosion resistance. The addition of Pd plays an important role in the performance adjustment and improvement of Zr-based BMG^[4,10]. However, there are few studies about the effect of Tm on the mechanical properties and corrosion resistance of metallic glass.

In this research, on the basis of the previous research on $\text{Zr}_{0.6336}\text{Cu}_{0.1452}\text{Ni}_{0.1012}\text{Al}_{0.12}$ BMG^[11-13], GFA, mechanical properties, and corrosion resistance of $(\text{Zr}_{0.6336}\text{Cu}_{0.1452}\text{Ni}_{0.1012}\text{Al}_{0.12})_{100-x}\text{Tm}_x$ ($x=0\sim 5$, at%) BMG were studied. The results provided basic knowledge and new ideas for the development of new Zr-based BMG as a structural material, which could meet the

Received date: September 29, 2020

Foundation item: National Natural Science Foundation of China (51861021, 51661016, 51571105, 51661017)

Corresponding author: Li Chunyan, Ph. D., Professor, School of Materials Science and Engineering, Lanzhou University of Technology, Lanzhou 730050, P. R. China, E-mail: licywz@163.com

Copyright © 2021, Northwest Institute for Nonferrous Metal Research. Published by Science Press. All rights reserved.

requirements of mechanical properties and corrosion resistance.

1 Experiment

Alloy ingots of $(\text{Zr}_{0.6336}\text{Cu}_{0.1452}\text{Ni}_{0.1012}\text{Al}_{0.12})_{100-x}\text{Tm}_x$ ($x=0\sim5$) BMG were prepared by levitation melting the constituent elements under the argon atmosphere: zirconium (Zr, purity of 99.7%), copper (Cu, purity of 99.99%), nickel (Ni, purity of 99.95%), aluminum (Al, purity of 99.99%), and thulium (Tm, purity of 99.99%). Each alloy ingot was remelted for three times to ensure the component homogeneity, and then suction cast in a copper mold to get rods with a diameter of 2 mm and a length of 70 mm. The alloy structure was examined by Bruker Axs D8 Advance X-ray diffraction (XRD, with Cu K α radiation) and transmission electron microscopy (TEM, FEI Talos F200X). The diffraction angle range 2θ was between 20° and 80° , and the step length was 0.02° . The thermodynamic character and crystallization behavior of small-sized specimens were measured by differential scanning calorimetry (DSC, NETZSCH DSC 204) under continuous argon flow atmosphere at a heating rate of $20\text{ K}\cdot\text{min}^{-1}$, and all the thermal parameters were determined with an accuracy of $\pm 1\text{ K}$. Mechanical tests of specimens were conducted by WDW-100D universal testing machine at room temperature with the strain rate of $1\times 10^{-4}\text{ s}^{-1}$, and the aspect ratio of specimens was about 2:1. At least three specimens were investigated by mechanical testing. The compressed fracture surfaces were observed by Quanta Feg450 field emission scanning electron microscope (SEM). The microhardness of specimens with diameters of 2 mm was measured by microhardness tester machine.

The corrosion behavior of this series of BMGs in service environment was determined by a three-electrode structure using the saturated calomel reference electrode, a platinum counter electrode, and a Zr-based BMG specimen as working electrode. Before the test, cylindrical BMG specimens with diameter of 2 mm were attached to the copper plate and inserted into the silicone grease with exposing surface area of 0.031 cm^2 . All specimens were gradually ground with sandpaper of 5000#, then polished, washed with absolute ethanol, and dried in cold air. NaCl solution of 3.5wt% was selected as the corrosion solution. The open circuit potential (OCP) curve of Zr-based BMGs in 3.5wt% NaCl was monitored for 1800 s by computer controlled CHI660E potentiostat. After OCP was stable, the dynamic polarization test was conducted at a potential scanning rate of 0.5 mV/s starting from -0.6 V until the passive film was broken. Moreover, the surface morphologies of different BMG specimens after polarization were observed through SEM, and the chemical composition of the passivation film surface was detected by energy dispersive spectrometer (EDS).

2 Results and Discussion

2.1 Structure and thermodynamic properties

XRD patterns of as-cast $(\text{Zr}_{0.6336}\text{Cu}_{0.1452}\text{Ni}_{0.1012}\text{Al}_{0.12})_{100-x}\text{Tm}_x$ ($x=0\sim5$) BMGs are shown in Fig.1, which consist of one broad diffuse peak of $2\theta=30^\circ\sim45^\circ$. With increasing the Tm content,

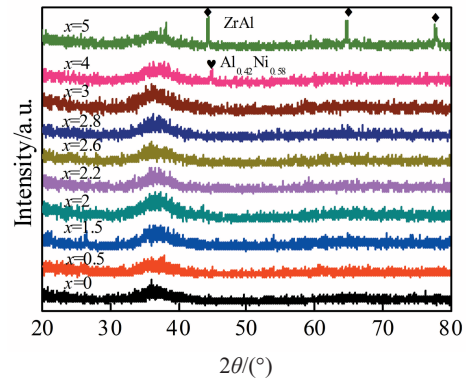


Fig.1 XRD patterns of as-cast $(\text{Zr}_{0.6336}\text{Cu}_{0.1452}\text{Ni}_{0.1012}\text{Al}_{0.12})_{100-x}\text{Tm}_x$ ($x=0\sim5$) alloys

the alloys with $x=0\sim3$ all show an amorphous structure which is further verified through TEM analysis of the alloy with $x=3$, as shown in Fig.2. The atoms are arranged irregularly and the diffraction spots are aureole, indicating that the structure of the alloy is completely amorphous. However, when $x=1.5$, weak crystallization peak appears at $2\theta=27^\circ$. When $x=4, 5$, the fine diffraction peaks corresponding to the $\text{Al}_{0.42}\text{Ni}_{0.58}$ phase and ZrAl phase can be observed, respectively. These results indicate that the alloy with $x=1.5, 4, 5$ has a composite structure of crystalline phase and the amorphous matrix phase.

Fig.3 shows DSC curves of $(\text{Zr}_{0.6336}\text{Cu}_{0.1452}\text{Ni}_{0.1012}\text{Al}_{0.12})_{100-x}\text{Tm}_x$ ($x=0\sim4$) alloys at heating rate of 20 K/min . The melting behavior of BMG was characterized by DSC curves. The glass transition temperature (T_g), onset temperature of crystallization (T_x), liquidus temperature (T_l), and melting temperature (T_m) are indicated by arrows in Fig.3. All thermal parameters of the alloy are summarized in Table 1. The results indicate that specimens exhibit the characteristic of glass transition, followed by a wide supercooled liquid region and different exothermic peaks caused by crystallization and melting endothermic peaks. In addition, the exothermic reaction of all alloys has only one peak, but there are two

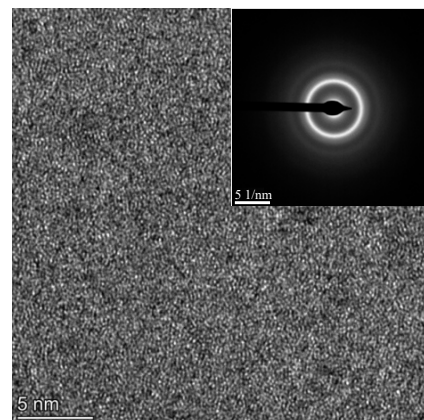


Fig.2 TEM image of $(\text{Zr}_{0.6336}\text{Cu}_{0.1452}\text{Ni}_{0.1012}\text{Al}_{0.12})_{100-x}\text{Tm}_x$ ($x=3$) alloy

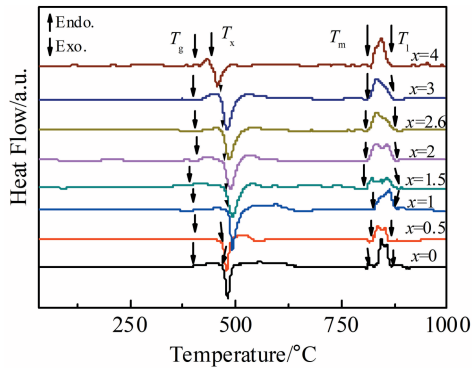


Fig.3 DSC curves of as-cast $(\text{Zr}_{0.6336}\text{Cu}_{0.1452}\text{Ni}_{0.1012}\text{Al}_{0.12})_{100-x}\text{Tm}_x$ ($x=0\sim 4$) alloys at heating rate of 20 K/min

endothermic peaks at low Tm content and only one endothermic peak at high Tm content ($x>2.6$), indicating that the alloy is an eutectic composition^[14]. Supercooled liquid region width $\Delta T_x = T_x - T_g$ and parameter γ ($\gamma = T_x / (T_g + T_l)$) are important indexes of thermal stability and GFA, respectively, as show in Table 1. With increasing the Tm content, the value of γ changes slightly. When $x=1.5$, the value of γ reaches the maximum value of 0.386. As the content of Tm continues to increase, the value of γ decreases, and then increases to 0.379 when $x=3$. Fig.4 shows the broken line chart of T_g , T_x , and ΔT_x value changing with Tm content. It can be observed that with increasing the Tm content, the change trends of T_g and T_x are similar. Meanwhile, ΔT_x increases from 95 °C for the alloys with $x=0$ to 100 °C for alloy with $x=3$, indicating that the thermal stability of the alloy with $x=3$ is optimal^[15]. The addition of a small amount of Tm improves the thermal stability of Zr-based metallic glasses. The alloy composition is located at or near the eutectic point, which is a necessary condition for obtaining the good thermal stability and GFA, i. e., the addition of Tm improves the thermodynamic properties of alloy.

The improvement of GFA can be explained by the three empirical rules of Inoue^[16]. Additionally, the difference of atomic size also leads to the GFA enhancement. In Zr-Cu-Ni-Al-Tm alloy system, the atomic radii of Zr, Cu, Ni, Al, and Tm are 0.160, 0.145, 0.124, 0.143, and 0.174 nm, respectively. The larger atomic size of Tm is helpful to increase the random

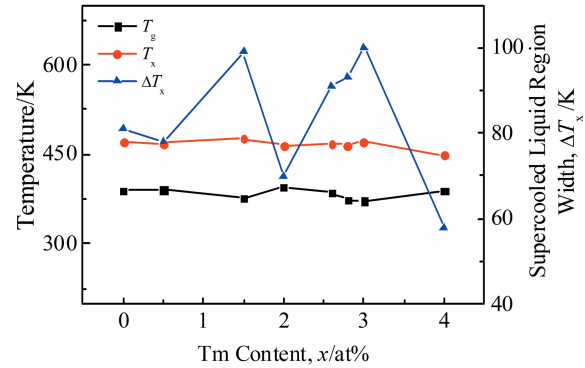


Fig.4 Thermodynamic curves of $(\text{Zr}_{0.6336}\text{Cu}_{0.1452}\text{Ni}_{0.1012}\text{Al}_{0.12})_{100-x}\text{Tm}_x$ ($x=0\sim 4$) alloys

packing density, which improves GFA^[17,18]. However, the positive mixing heat may reduce the bulk density and deteriorate the strong atom bonding structure of the alloy when Tm is excessive ($x>3$). Therefore, GFA of the alloy begins to decrease when $x>3$, which is consistent with the experiment results.

2.2 Mechanical properties

Fig. 5a shows the compression stress-strain curves and partially enlarged diagrams of $(\text{Zr}_{0.6336}\text{Cu}_{0.1452}\text{Ni}_{0.1012}\text{Al}_{0.12})_{100-x}\text{Tm}_x$ ($x=0\sim 5$) alloys. It is found that all specimens firstly undergo the elastic deformation and then yield, showing a certain degree of plastic deformation before the fracture. Some specimens show good plasticity. The mechanical properties of structural materials are usually indicated by the compressive fracture strength (σ_p) and compressive plasticity (ε_p) of the alloy, as listed in Table 2. The compressive fracture strength of the alloy decreases as the Tm content increases. However, when Tm content increases to 3at%, the compressive fracture strength of the alloy reaches the maximum value of 1669 MPa. The remarkable compressive plasticity of 21.01% occurs in the alloy with $x=3$, which is much higher than that in the alloy with $x=0$ (5.90%). The results show that the compressive plasticity of the alloy is improved by adding new elements with positive heats of mixture with other elements^[19,20]. Therefore, the fracture strength and compression plasticity of BMGs are significantly improved by proper addition of Tm. The addition of Tm results in the inhomogeneity of free volume distribution in the amorphous phase, which is considered to be the starting position and barrier layer of the shear band, and eventually leads to the nucleation and branching of the shear band, thereby improving ε_p of the alloy^[10,21,22]. Similarly, the increase of fracture strength is closely related to the addition of new elements: the addition of new elements can enhance the mismatch of different atomic sizes among the main elements in the alloy, resulting in the increase of fracture strength^[23].

From Fig. 5b and 5c, it can be found that the deformation mechanism of two different deformation stages of alloy is completely different. There are many serrations in the curve of plastic deformation part consisting of the rising part of stress

Table 1 GFA parameters of $(\text{Zr}_{0.6336}\text{Cu}_{0.1452}\text{Ni}_{0.1012}\text{Al}_{0.12})_{100-x}\text{Tm}_x$ ($x=0\sim 4$) alloys

x	$T_g/^\circ\text{C}$	$T_x/^\circ\text{C}$	$T_m/^\circ\text{C}$	$T_l/^\circ\text{C}$	$\Delta T_x/^\circ\text{C}$	γ
0	390	471	836	861	81	0.376
0.5	391	469	824	858	78	0.375
1	388	466	819	868	77	0.276
1.5	377	476	812	873	99	0.386
2	395	465	833	872	70	0.367
2.6	387	469	816	872	91	0.375
3	372	472	817	874	100	0.379
4	390	448	821	857	58	0.352

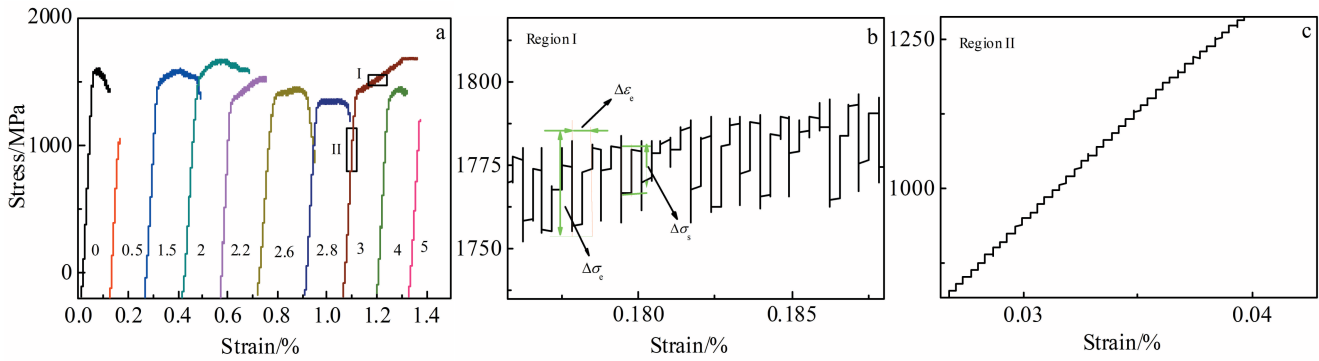


Fig.5 Compressive stress-strain curves of $(Zr_{0.6336}Cu_{0.1452}Ni_{0.1012}Al_{0.12})_{100-x}Tm_x$ ($x=0\sim5$) alloys (a); amplification of region I (b) and elastic deformation of region II (c) in Fig.5a

Table 2 Mechanical properties of $(Zr_{0.6336}Cu_{0.1452}Ni_{0.1012}Al_{0.12})_{100-x}Tm_x$ ($x=0\sim5$) alloys

x	$\varepsilon_p/\%$	σ_s/MPa	σ_e/MPa	σ_f/MPa
0	5.90	1539	1675	1493
0.5	0	1027	1027	1027
1.5	10.11	1467	1632	1528
2	13.31	1499	1688	1584
2.2	14.10	1370	1531	1557
2.6	9.01	1377	1421	1423
2.8	13.10	1330	1349	1301
3	21.01	1414	1669	1669
4	1.02	1159	1159	1159
5	0	1208	1208	1208

under elastic loading and the decreasing part of stress caused by the slip of shear band. The variation of serrated flow of plastic deformation was investigated through analyzing the stress drop ($\Delta\sigma_s$) and stress rise ($\Delta\sigma_e$), as shown in Fig.5b. The strain required for stress rise is $\Delta\varepsilon_e$. Fig. 6 shows the stress drop $\Delta\sigma_s$ curves, and plastic deformation caused by serration flow in the plastic strain stage of Zr-based BMGs under deformation of 0.2% was selected. It can be seen that the stress drop of the alloys ($x=0, 4$) with poor plasticity fluctuates with increasing the deformation. Meanwhile, the increase of the stress drop shows that it is exceedingly difficult to produce serrations, and stress drop needs more energy to produce serrations, which also increases the probability of fracture. Alloys ($x=2, 3$) with better plasticity ($\varepsilon_p > 5\%$) present a more stable stress drop with increasing the deformation, and the fluctuation range is smaller, indicating that with increasing the Tm content, the stress drop is increased and then decreased. In essence, the plastic deformation of the alloy is the combination of the elastic deformation of specimen and the slip of shear band. The elastic deformation is attributed to the slid and disappearance of the shear band^[24].

The variation curves of microhardness and yield strength of BMG specimens are shown in Fig.7. It can be seen that when $x \leq 3$, the yield strength and microhardness have the similar

change trend. With increasing the Tm content, the microhardness changes slightly, reaches the first peak value of 4641 MPa at $x=2$, then decreases, and finally increases to the maximum value of 4674 MPa at $x=4$. The yield strength fluctuates greatly after $x=2$. As shown in Fig.5, the plasticity of the specimen of $x=3$ reaches the maximum of 21.01%, while its microhardness reaches the minimum value of 4430 MPa. Generally, the decrease of microhardness is accompanied by the increase of plasticity and toughness, which is also confirmed by the change of compression plasticity.

Fig. 8 and Fig. 9 show the fracture morphologies and shear band characteristics of $(Zr_{0.6336}Cu_{0.1452}Ni_{0.1012}Al_{0.12})_{100-x}Tm_x$ ($x=0\sim4$) BMGs after compression tests, respectively. It is well known that the plasticity difference of BMG is attributed to the vein morphology of fracture surface and the density of shear band distribution. Generally, the fracture occurs in the plane of the maximum shear stress of BMG, which is about 45° away from the direction of compression load. As shown in Fig. 8, the fracture surface of as-cast specimen shows different vein shapes during stress loading. For the specimen with $x=0$ (Fig.8a), although there are many intensive veins, the diameter of veins is smaller and the distribution is more inhomogeneous compared with the morphology of specimen with $x=3$. The alloy with $x=0.5$ shows very few river veins in Fig.8b. The as-cast alloy with $x=3$ has higher vein density and more regular veins than other alloys do, which corresponds with the excellent plasticity of alloy with $x=3$. Owing to the high elastic energy accumulated in the shear band of the specimen before fracture, the temperature of the fracture surface increases rapidly, and then the molten droplets are formed^[25,26], as show in Fig. 8c and 8d. These droplets can prove the adiabatic heating during deformation of BMG and explain their localization^[27]. However, as shown in Fig. 8f, there are a lot of smooth, rough, and plane cracks on the fracture surface, which is a typical brittle fracture feature of massive metallic glass. This phenomenon shows that the plasticity of Zr-based BMG can be improved by adding a proper amount of Tm element, but it can be reduced by adding excessive Tm element.

It can be manifested from Fig. 9 that the shear band of

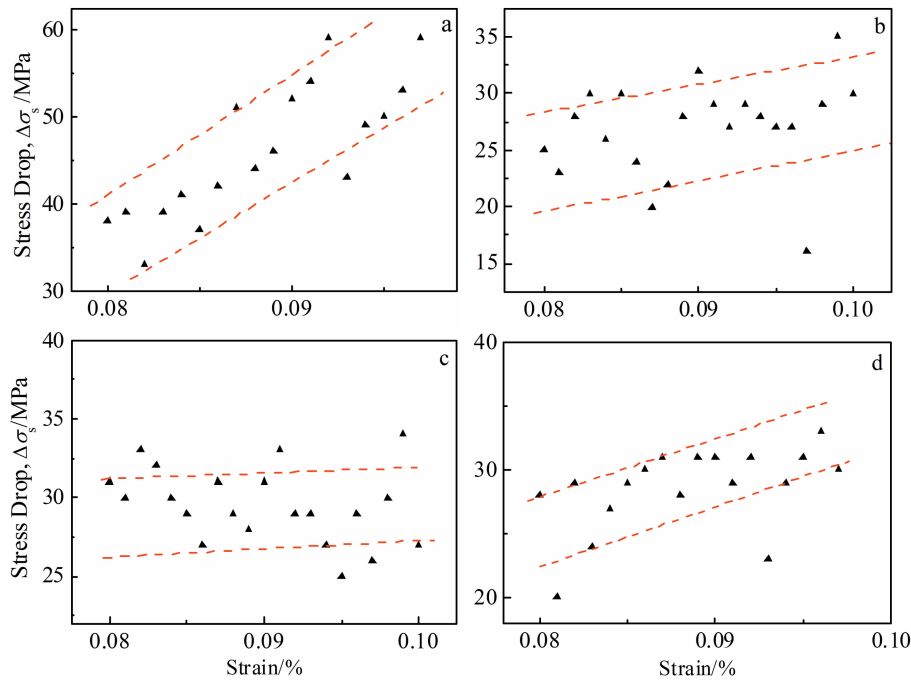


Fig.6 Stress drop-strain curves of $(\text{Zr}_{0.6336}\text{Cu}_{0.1452}\text{Ni}_{0.1012}\text{Al}_{0.12})_{100-x}\text{Tm}_x$ alloys: (a) $x=0$, (b) $x=2$, (c) $x=3$, and (d) $x=4$

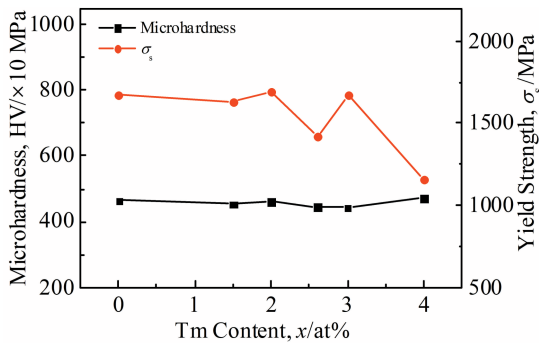


Fig.7 Relationship of microhardness and yield strength with Tm content of $(\text{Zr}_{0.6336}\text{Cu}_{0.1452}\text{Ni}_{0.1012}\text{Al}_{0.12})_{100-x}\text{Tm}_x$ alloys ($x=0\sim 4$)

fracture specimen is mainly composed of main shear band, secondary shear band, and root shear band. In general, the density and distribution type of the shear band of the specimen determine the plasticity of BMG. As shown in Fig. 9a, the specimen of $x=0$ shows that there are only a few main shear bands and secondary shear bands on the side of the specimen along one single direction. The single direction and small quantity of shear bands lead to excessive stress concentration, resulting in the crack propagation along the single shear band and eventually leading to brittle fracture of the specimens. Fig. 9b and 9c indicate the shear band morphologies of specimen of $x=3$ obtained from the first and repeated tests, respectively. Overall, there are a host of main shear bands, secondary shear bands, and root shear bands in the shear band morphology, which are unique for metallic glass, especially in front of the propagation direction of the

main shear band, as shown in Fig. 9b. There are many relatively dense whisker bands lying between the secondary shear regions, as shown in Fig. 9c. As shown in Fig. 9d, the shear band morphology of alloy of $x=4$ shows that the number of primary shear bands and secondary shear bands is significantly less, which also proves the brittle fracture. In addition, there are crossing, branching, and other transfer phenomena, including the secondary shear bands or root shear bands decomposed from the main shear bands. The existence of these high-density secondary shear bands and root shear bands can make the crack propagate along the multiple shear bands, which avoids the brittle fracture caused by stress concentration. The existence of high-density shear band proves the rheological behavior of BMG. The plasticity and strength of alloys strongly depend on the high-density shear band, which can effectively prevent cracks from propagating along one direction. This is a fair explanation for the excellent plasticity and strength of alloy of $x=3$. When the Tm content increases, a smoother area without plasticity or the area with vein pattern can be observed, illustrating that the plasticity of BMG decreases, which is consistent with the result of stress-strain curves in Fig. 5.

2.3 Electrochemical behavior

In addition to the mechanical properties, it is important to evaluate the effect of Tm addition on the corrosion behavior of as-cast $(\text{Zr}_{0.6336}\text{Cu}_{0.1452}\text{Ni}_{0.1012}\text{Al}_{0.12})_{100-x}\text{Tm}_x$ ($x=0\sim 5$) alloys. Firstly, OCP of specimens with different components was measured. Theoretically, the corrosion trend of Zr-based BMGs can be predicted by OCP. It is noticed that no obvious transient phenomenon was observed during the evolution of OCP. The OCP value is increased with increasing the

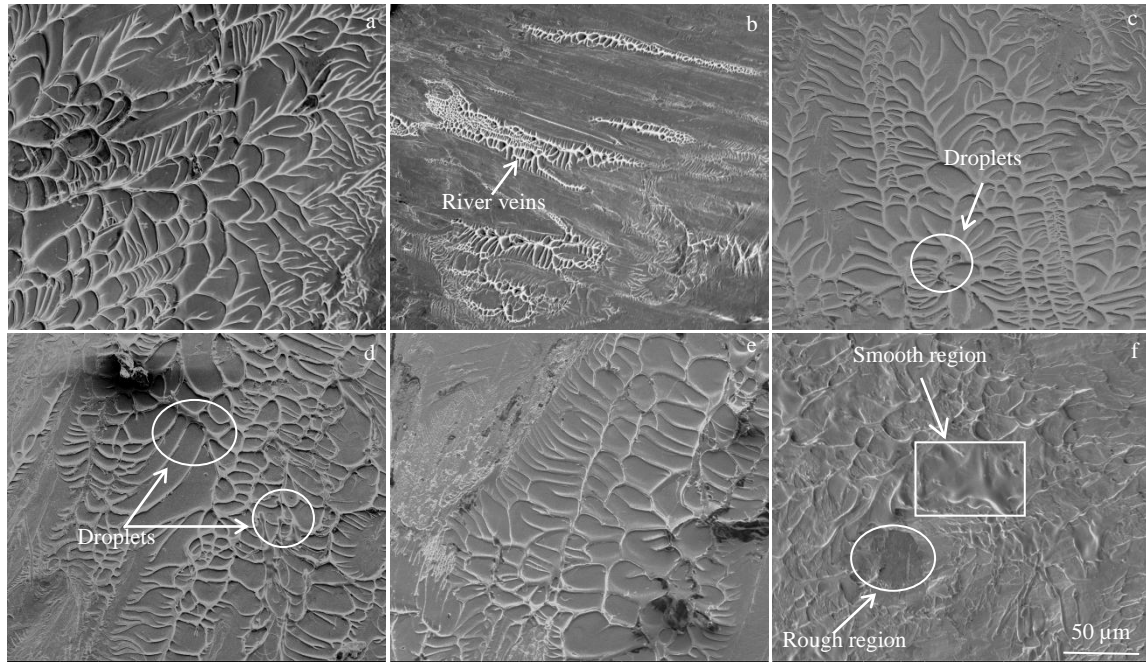


Fig.8 SEM images of fracture morphologies of $(Zr_{0.6336}Cu_{0.1452}Ni_{0.1012}Al_{0.12})_{100-x}Tm_x$ alloys: (a) $x=0$, (b) $x=0.5$, (c) $x=1.5$, (d, e) $x=3$, and (f) $x=4$

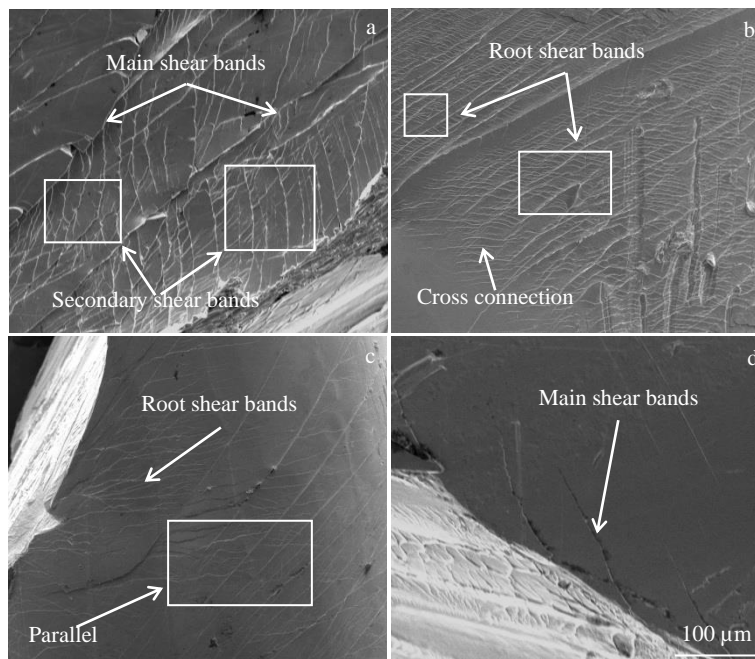


Fig.9 SEM images of compression side shear band of $(Zr_{0.6336}Cu_{0.1452}Ni_{0.1012}Al_{0.12})_{100-x}Tm_x$ alloys: (a) $x=0$, (b) $x=3$ from the first compression test, (c) $x=3$ from the repeated compression test, and (d) $x=4$

immersion time in 3.5wt% NaCl solution, indicating that all Zr-based BMGs are passivated spontaneously.

The corrosion behavior of Tm-added Zr-based BMGs in 3.5wt% NaCl solution was studied by potentiodynamic polarization. As shown in Fig.10, all specimens are passivated spontaneously by anodic polarization with a wide passivation range, and then suffer pitting corrosion at a relatively high

potential. Although the polarization behavior of the tested specimen is similar, the polarization curve clearly records the significant difference of corrosion resistance of different alloys in NaCl solution. Important electrochemical parameters including pitting potential (E_{pit}), corrosion potential (E_{corr}), and corrosion current density (I_{corr}) attained from potentiodynamic polarization curves are summarized in Table 3. E_{pit} is a key

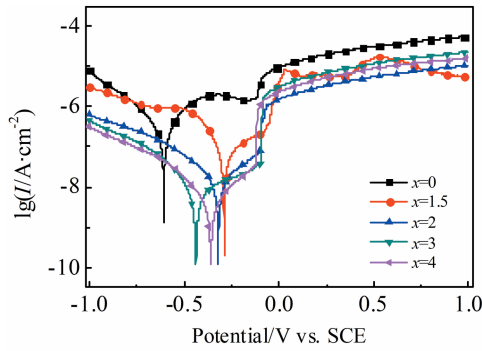


Fig.10 Potentiodynamic polarization curves ($\lg I-E$) of as-cast $(\text{Zr}_{0.6336}\text{Cu}_{0.1452}\text{Ni}_{0.1012}\text{Al}_{0.12})_{100-x}\text{Tm}_x$ ($x=0\sim 4$) alloys in 3.5wt% NaCl solution at room temperature

Table 3 Electrochemical parameters (E_{corr} , I_{corr} , E_{pit}) derived from potentiodynamic polarization curves of as-cast $(\text{Zr}_{0.6336}\text{Cu}_{0.1452}\text{Ni}_{0.1012}\text{Al}_{0.12})_{100-x}\text{Tm}_x$ ($x=0\sim 4$) alloys

x	E_{corr}/V	$I_{\text{corr}}/\text{A}\cdot\text{cm}^{-2}$	E_{pit}/V
0	-0.607	2.43×10^{-7}	-0.10
1.5	-0.289	8.63×10^{-8}	-0.05
2	-0.321	1.78×10^{-8}	-0.09
3	-0.439	7.01×10^{-9}	-0.08
4	-0.361	4.13×10^{-9}	-0.12

parameter to evaluate the corrosion resistance of materials: a larger E_{pit} represents a smaller probability of pitting corrosion. It can be seen from Table 3 that with increasing the Tm

content, the value of E_{pit} shows an increasing trend overall, although the E_{pit} value of specimen of $x=1.5$ is slightly higher than that of specimen of $x=3$, which indicates the optimal corrosion resistance actually appears when $x=1.5$. The results show that the pitting corrosion resistance of Zr-based BMG decreases when the amount of Tm is insufficient. Although BMG with 3at% Tm has the best mechanical properties, its corrosion resistance is not optimal. The reason may be that the further addition of Tm element can easily generate stable oxides, which promotes the formation of passive film on the surface of the specimen and leads to pitting corrosion^[28].

Moreover, the corrosion morphologies of Zr-based BMGs are shown in Fig. 11. Obviously, pitting corrosion appears on the surface of Zr-based BMGs ($x=0, 1.5, 2, 3$). It can be observed that the surface of the alloy of $x=0$ (Fig. 11a) has obvious corrosion pits with a size of about 12 μm . When Tm content increases to 1.5at%, the number of corrosion pits are significantly reduced (Fig. 11b), which indicates that the addition of Tm has a positive effect on the pitting resistance of Zr-based BMGs. However, as shown in Fig. 11c, when Tm content increases to 2at%, many corrosion pits with the size of about 20 μm appear, which indicates that the passivation film is broken. When the Tm content increases to 3at%, smaller pitting (compared with the pitting of alloy of $x=2$) can be observed, as indicated by the white circles in Fig. 11d. In the meantime, for the large corrosion pits of the alloy with $x=2$, the alloy surface was analyzed by EDS surface scanning, and the result is shown in Fig. 12. Besides Zr, Cu, Ni, Al, and Na elements, Cl element was also detected and its content is 1.7at%, which confirms that Cl⁻ causes the rupture of passi-

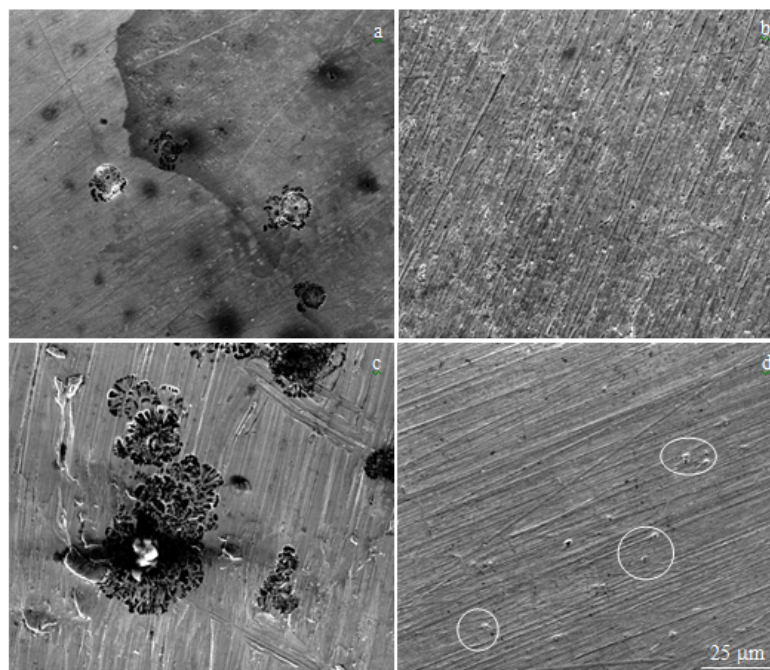


Fig.11 SEM images of corrosion morphologies of $(\text{Zr}_{0.6336}\text{Cu}_{0.1452}\text{Ni}_{0.1012}\text{Al}_{0.12})_{100-x}\text{Tm}_x$ alloys after potentiodynamic potential tests in 3.5wt% NaCl solutions: (a) $x=0$, (b) $x=1.5$, (c) $x=2$, and (d) $x=3$

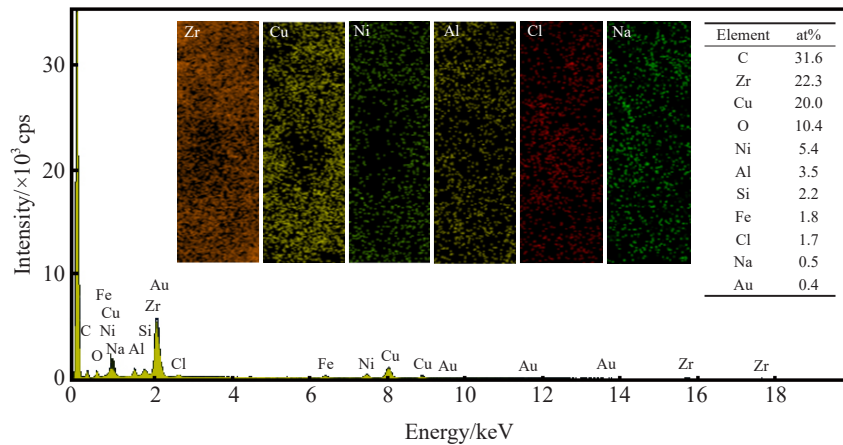


Fig.12 EDS analysis results of surface films of as-cast $(Zr_{0.6336}Cu_{0.1452}Ni_{0.1012}Al_{0.12})_{98}Tm_2$ alloy at corrosion region

vation film and severe pitting, leading to the poor corrosion resistance^[5]. However, none Cl was detected on the surface of alloy of $x=1.5$, indicating that the alloy has a complete passivation film and the addition of an appropriate amount of Tm is beneficial to improving the corrosion resistance. Generally, Zr-based BMGs can easily form passive films spontaneously under oxidizing conditions. However, Cl⁻ replaces oxides and is adsorbed in the passive film in Cl⁻ containing solutions, resulting in the formation of soluble metal chlorides. As a result, pitting corrosion occurs in the exposed part of the metal until local corrosion appears^[29]. Overall, the addition of an appropriate amount of Tm can improve the corrosion resistance and passivation film integrity. The inconsistency between excellent GFA and corrosion resistance can be attributed to the amorphous structure and different chemical composition.

3 Conclusions

1) The glass forming ability (GFA), thermal stability, and plastic strain are improved by adding 3at% Tm into Zr-Cu-Ni-Al alloy. The maximum supercooled liquid region width ΔT_x of the prepared alloy is 100 K, compressive plasticity at room temperature is 21.01%, and the value of γ is 0.379. Compared with the properties of the alloy without Tm, the compressive plasticity at room temperature and fracture strength increases from 5.90% and 1493 MPa to 21.01% and 1669 MPa, respectively.

2) Electrochemical tests show that the effect of Tm addition on the corrosion resistance of Zr-based BMG is not similar to that on mechanical properties. It is found that the alloy with 1.5at% Tm has excellent corrosion resistance. With increasing the Tm content within a proper range, the passivation ability and corrosion resistance of other alloys are increased significantly. In general, the inconsistency between excellent GFA and corrosion resistance can be attributed to the amorphous structure and different chemical composition.

References

- Schuh C, Hufnagel T, Ramamurty U et al. *Acta Materialia*[J], 2007, 12(55): 4067
- Han Jiajia, Wang Cuiping, Kou Shengzhong et al. *Transactions of Nonferrous Metals Society of China*[J], 2013, 23(1): 148
- Hu Q, Fu M W, Zeng X R et al. *Materials & Design*[J], 2014, 64: 301
- Han Kaiming, Wang Yingmin, Qiang Jianbing et al. *Journal of Non-Crystalline Solids*[J], 2019, 520: 119 442
- Shi Hongqi, Zhao Wenbo, Wei Xinwen et al. *Journal of Alloys and Compounds*[J], 2020, 815: 152 636
- Huo J T, Zhao D Q, Bai H Y et al. *Journal of Non-Crystalline Solids*[J], 2013, 359: 1
- Li Jiawei, Law Jia Yan, Huo Juntao et al. *Journal of Alloys and Compounds*[J], 2015, 644: 346
- Kou X H, Luo Q, Dinh P N et al. *Journal of Alloys and Compounds*[J], 2017, 699: 591
- Li Jun, Xue Lin, Yang Weiming et al. *Intermetallics*[J], 2018, 96: 90
- Hua Nengbin, Chen Wenzhe. *Journal of Alloys and Compounds* [J], 2017, 693: 816
- Li Chunyan, Kou Shengzhong, Zhao Yanchun et al. *Chinese Journal of Rare Metals*[J], 2015, 39(4): 300 (in Chinese)
- Li Chunyan, Kou Shengzhong, Zhao Yanchun et al. *Scientia Sinica: Physica, Mechanica & Astronomica*[J], 2012, 42(6): 571 (in Chinese)
- Li Chunyan, Zhu Fuping, Ding Juanqiang et al. *Rare Metal Materials and Engineering*[J], 2020, 49(10): 3353
- Si Jiajia, Du Chenxi, Wang Tan et al. *Journal of Alloys and Compounds*[J], 2018, 741: 542
- Zhang Wei, Miao Haitao, Li Yanhui et al. *Journal of Alloys and Compounds*[J], 2017, 707: 57
- Inoue A. *Acta Materialia*[J], 2000, 48(1): 279
- Guo S, Liu C T. *Progress in Natural Science: Materials International*[J], 2011, 21(6): 433
- Zhang Z B, Liang X B, Chen Y X et al. *Materials and Corrosion* [J], 2014, 65(9): 919

- 19 Lee M H, Lee J Y, Bae D H et al. *Intermetallics*[J], 2004, 12(10-11): 1133
- 20 Sun Y D, Chen Q R, Li G Z et al. *Journal of Alloys and Compounds*[J], 2014, 584: 273
- 21 Park E S, Kyeong J S, Kim D H. *Materials Science and Engineering A*[J], 2007, 449: 225
- 22 Liu X J, Chen G L, Hui X et al. *Applied Physics Letters*[J], 2008, 93(1): 11 911
- 23 Zhang T, Inoue A. *Materials Transactions*[J], 2002, 43(6): 1367
- 24 Zhang Wei, Kou Shengzhong, Ai Yajun et al. *The Chinese Journal of Nonferrous Metals*[J], 2017, 27(12): 2527 (in Chinese)
- 25 Liu C T, Heatherly L, Horton J A et al. *Metallurgical and Materials Transactions A*[J], 1998, 29(7): 1811
- 26 Li Chunyan, Yin Jinfeng, Ding Juanqiang et al. *Materials Science and Technology*[J], 2018, 34(15): 1887
- 27 Lewandowski J J, Greer A L. *Nature Materials*[J], 2005, 5(1): 15
- 28 Wang B, Xu K K, Shi X H et al. *Journal of Alloys and Compounds*[J], 2019, 770: 679
- 29 Burstein G T, Liu C, Souto R M et al. *Corrosion Engineering, Science and Technology*[J], 2004, 39(1): 25

Tm对锆基块体非晶合金力学性能和腐蚀性能的影响

王顺平^{1,2}, 李春燕^{1,2}, 李金玲¹, 王海博¹, 寇生中^{1,2}

(1. 兰州理工大学 省部共建有色金属先进加工与再利用国家重点实验室, 甘肃 兰州 730050)

(2. 兰州理工大学 材料科学与工程学院, 甘肃 兰州 730050)

摘要: 采用铜模负压吸铸工艺制备了 $(Zr_{0.6336}Cu_{0.1452}Ni_{0.1012}Al_{0.12})_{100-x}Tm_x$ ($x=0\sim 5$, 原子分数) 块体金属玻璃 (BMG) 合金, 研究了Tm对合金力学性能和抗腐蚀性能的影响。结果表明, 当Tm含量增加到3%时, 其玻璃形成能力 (GFA) 和压缩塑性显著提高, 但过量Tm会降低GFA。 $x=3$ 时合金的最大过冷液相区宽度为100 K, 抗压强度为1669 MPa, 塑性应变为21.01%, 远高于 $Zr_{0.6336}Cu_{0.1452}Ni_{0.1012}Al_{0.12}$ BMG的各项性能 (67 K、1439 MPa和5.90%)。然而, 电化学测试结果表明, $x=3$ 时的合金在3.5% (质量分数) NaCl溶液中的耐腐蚀性不佳, 且其耐腐蚀性和力学性能随Tm含量的变化趋势与预期不同。可能是由于过量添加稀土元素Tm, 容易形成更多的氧化物, 导致点蚀加剧。进一步添加Tm可以提高Zr基BMG钝化膜的完整性和耐点蚀性能, 但力学性能不理想。

关键词: Zr基非晶合金; 力学性能; 腐蚀性能; Tm

作者简介: 王顺平, 男, 1993年生, 硕士, 兰州理工大学材料科学与工程学院, 甘肃 兰州 730050, E-mail: shunping0826@163.com